Available online at www.sciencedirect.com
ScienceDirect
Journal of Sound and Vibration 321 (2009) 704–720
JOURNAL OF SOUND AND VIBRATION
www.elsevier.com/locate/jsvi

Substructure synthesis method for a nonlinear structure with a sliding mode condition

Dae-Kwan Kim[a], Min-Su Lee[b], Jae-Hung Han[c,*]

[a]*COMS Systems Department, Korea Aerospace Research Institute, 115 Gwahangno, Yuseong-gu, Daejeon 305-333, Republic of Korea*
[b]*Mechatronics Center, Institute of Industrial Technology, Samsung Heavy Industry, 103-28 Munji-dong, Yuseong-gu, Daejoen 305-380, Republic of Korea*
[c]*Department of Aerospace Engineering, KAIST, 335 Gwahangno, Yuseong-gu, Daejeon 305-701, Republic of Korea*

Received 20 January 2007; received in revised form 26 April 2008; accepted 27 September 2008
Handling Editor: L.G. Tham
Available online 18 November 2008

Abstract

The component mode synthesis (CMS) method is widely used to establish reduced dynamic models of complex structures so that iterative problems such as flutter analyses can be efficiently analyzed with reasonable cost and time. In the present study, a structural coupling method is developed for the dynamic analysis of a nonlinear structure consisting of substructures connected by nonlinear interfaces such as nonlinear hinge joints or sliding mode conditions. In order to verify the coupling method extended to consider the hinge joints, a numerical plate model consisting of two substructures and torsional springs is synthesized, and its modal parameters are compared with analysis data. The extended coupling method is further improved to consider the sliding mode condition. The improved coupling method is applied to a three-substructure-model with nonlinearity of sliding lines between the substructures. Finally, using the proposed coupling method, a dynamic model of a tilting structure consisting of two substructures with sliding line conditions is synthesized, and its dynamic characteristics are investigated. The analysis results show that the improved coupling method is effectively applicable to the dynamic analysis of a nonlinear structure with the sliding mode condition.

1. Introduction

Most practical engineering structures are complicated with distributed or concentrated structural nonlinearities. For example, a deployable missile control fin has a nonlinear hinge joint that consists of a torsional spring, a compression spring, and several stoppers. Because of wear and manufacturing tolerance, the hinge has some structural nonlinearities such as preload, free-play, asymmetric bilinear stiffness, hysterisis, and coulomb damping [1]. Another example is a pantograph tilting system consisting of a pantograph and a tilting structure. The pantograph tilting system is currently being used in tilting trains, which are becoming the standard internationally, especially in Europe. The car body of a tilting train moving on a curved line is tilted inward to compensate the centrifugal force, as shown in Fig. 1. Therefore, the speed and run can be increased

*Corresponding author. Tel.: +82 42 869 3723; fax: +82 42 869 3710.
E-mail address: jaehunghan@kaist.ac.kr (J.-H. Han).

0022-460X/$ - see front matter © 2008 Elsevier Ltd. All rights reserved.
doi:10.1016/j.jsv.2008.09.052

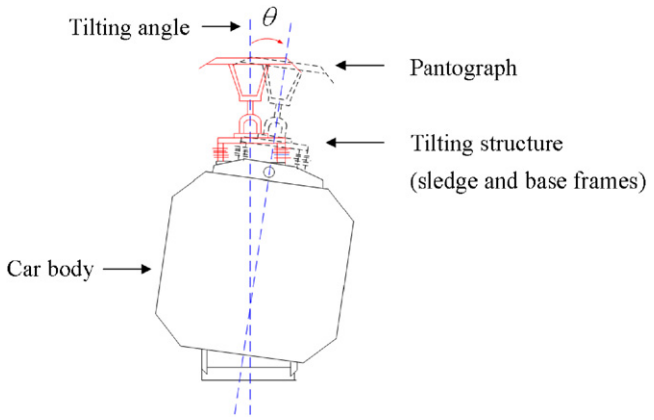

Fig. 1. Schematic diagram of pantograph tilting structure.

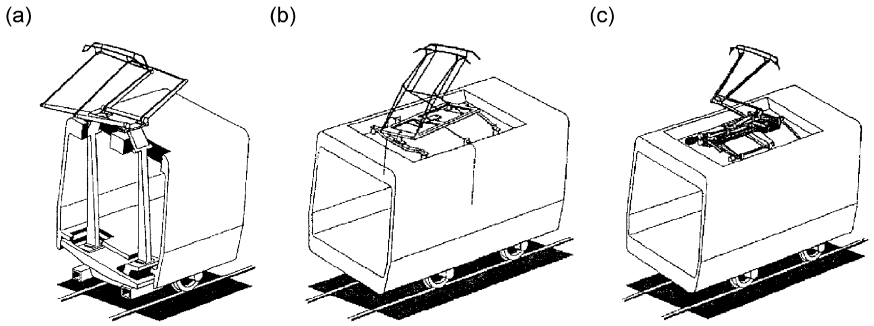

Fig. 2. Pantograph tilting devices: (a) bogie mounted pantograph; (b) roof mounted passive pantograph; and (c) roof mounted active pantograph [2].

on conventional curved lines whereas normally speed reduction would be necessary. In order to maintain a reliable electrical energy supply from the catenary to the train by means of the contact between the pantograph and catenary cables, even when the train is at maximum inclination, the train must have an anti-tilt mechanism such as a bogie mounted pantograph or roof mounted passive or active pantographs, as shown in Fig. 2. The roof mounted active tilting structure, which consists of base and sledge frames driven by electromechanical actuators, has been widely used and developed. Despite disadvantages such as more complex failure modes and new design, this structure allows for no loss of passenger seats and full compensation of the suspension roll effect while being of low weight [2]. The pantograph tilting systems also have some structural nonlinearities because of worn or loose hinges of the pantograph, and a sliding mode condition between the sledge and base frames. These nonlinearities cannot be completely eliminated, and exert significant effects on the static and dynamic characteristics of the pantograph tilting structure. Therefore, it is necessary to establish an accurate structural dynamic model to predict or control the nonlinear dynamic systems. However, considerable computational effort is required to perform dynamic analyses of many practical engineering problems by making use of full-order nonlinear finite element models, especially when iterate analyses are required such as time-domain nonlinear flutter analyses or structural optimal design.

In general, most practical engineering structures are complicated and may have some nonlinearities. The information about the position of structural nonlinearity offers opportunities to separate the total structure into linear and nonlinear components, so that they can be analyzed and designed independently. In order to reduce the number of coordinates in a dynamic analysis of a complex structure, the component mode synthesis (CMS) techniques are popularly used in structural dynamic applications for combining substructures or components represented with reduced degrees of freedom (dof). Numerous studies on substructure synthesis methods have been reported. Hunn [3] introduced the first partial modal coupling method. Hurty [4] assumed

that the motion of each substructure could be expressed by a linear combination of some component modes consisting of rigid-body modes, constraint modes, and normal modes. Craig and Bampton [5] treated the displacements of substructures as being composed of constraint modes and normal modes. This model is known popularly as the fixed interface CMS method. Craig and Chang [6,7] developed free and hybrid interface CMS methods employing free interface substructure normal modes supplemented by reduced flexibility to account for the effects of residual modes. Meirovitch and Hale [8,9] introduced admissible functions and vectors to represent the motion of each substructure. Kapel et al. [10–12] suggested fictitious masses loaded at interface coordinates of a central substructure of which the connection to the additional substructure is statically determinate. Bourquin and d'Hennezel [13] proposed a reduction procedure based on the use of interface modes to reduce the number of interface coordinates in the fixed interface CMS method. Tran [14] extended this procedure to the free and hybrid interface methods. Bladh et al. [15] investigated the numerical instability of the free interface CMS methods due to matrix ill-conditioning and proposed a stabilized free interface CMS method. Apiwattanalunggarn et al. [16] extended the fixed interface linear CMS method to nonlinear structures by using fixed interface nonlinear normal modes. This approach is valid as long as the coupling between substructures is relatively weak. Kim et al. [17] extended the Craig–Bampton method to consider concentrated nonlinear hinge springs and then established a nonlinear dynamic model of a deployable missile control fin. Shanmugam and Padmanabhan [18] developed a hybrid CMS method by combining the fixed interface method and the free interface method, and carried out a rotordynamic analysis.

Over the years studies on train pantograph systems have mostly focused on active control of the pantographs in order to exert constant contact forces between catenaries and pantographs [19–21] as well as modeling and analyses of the dynamic interactions of the catenary–pantograph systems in conventional high speed trains [22–25]. As far as the authors are aware, modeling and dynamic analysis of pantograph tilting systems have not been documented in the open literature.

In the present study, the extended Craig–Bampton method is improved to take into account not only the concentrated structural nonlinearities but also the sliding mode condition. In order to verify the extended coupling method, a numerical plate model consisting of two substructures and seven torsional springs is synthesized. The extended method is then further improved to consider the sliding mode condition. The improved coupling method is applied to a three-substructure-model with structural nonlinearity of sliding lines between the substructures, and the coupled structural model is verified with dynamic results. Finally, a nonlinear reduced model of a pantograph tilting structure is established by using the proposed coupling method, and the dynamic characteristics are investigated.

2. Substructure synthesis for hinge joints

The substructure synthesis method, extended to consider concentrated nonlinear hinge joints, is summarized in this section. In order to verify the method, a numerical plate model with two substructures and seven torsional springs is synthesized by using the extended method, and its modal parameters are compared with analysis data.

2.1. CMS method

To analyze the dynamic characteristics of a complex structure by using the substructure synthesis method, it is necessary to divide the whole structure into a limited number of substructures. Each substructure is connected to at least one of the other substructures, as shown in Fig. 3.

For an arbitrary linear undamped substructure, the equations of motion of a substructure A are written as

$$\begin{bmatrix} M_{RR} & M_{RI} \\ M_{RI}^{\mathrm{T}} & M_{II} \end{bmatrix} \begin{Bmatrix} \ddot{u}_R \\ \ddot{u}_I \end{Bmatrix} + \begin{bmatrix} K_{RR} & K_{RI} \\ K_{RI}^{\mathrm{T}} & K_{II} \end{bmatrix} \begin{Bmatrix} u_R \\ u_I \end{Bmatrix} = \begin{Bmatrix} 0 \\ F_I \end{Bmatrix} \tag{1}$$

where $\{F_I\}$ is the vector of forces applied at the interface coordinates by the adjoining substructure. The mass and stiffness matrices M and K and the displacement and force vectors u and F are partitioned according to the interior (R) and interface (I) coordinates of the substructure.

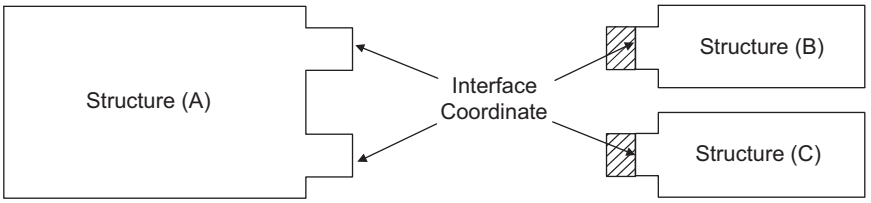

Fig. 3. A scheme of separate structure analysis.

The basic assumption in the CMS method is that the displacement of each substructure can be represented by a linear combination of some normal and constraint modes as follows:

$$\begin{Bmatrix} u_R \\ u_I \end{Bmatrix} = \begin{bmatrix} \Psi_N & \Psi_C \\ 0 & I \end{bmatrix} \begin{Bmatrix} \xi_R \\ \xi_I \end{Bmatrix} \tag{2}$$

where $[\Psi_N]$, $[\Psi_C]$, and $\{\xi_R \ \ \xi_I\}^{\mathrm{T}}$ are the normal modes, the constraint modes, and the vector of independent generalized displacements, respectively. These modes can be obtained by the eigenvalue problem and the static equilibrium equation described in detail in Refs. [5,17].

The substitution of Eq. (2) into Eq. (1), and pre-multiplication by the transformation matrix of Eq. (2), gives

$$\begin{bmatrix} m_{RR}^{(A)} & m_{RI}^{(A)} \\ m_{RI}^{(A)\mathrm{T}} & m_{II}^{(A)} \end{bmatrix} \begin{Bmatrix} \ddot{\xi}_R^{(A)} \\ \ddot{\xi}_I^{(A)} \end{Bmatrix} + \begin{bmatrix} \omega_R^{2(A)} & 0 \\ 0 & k_I^{(A)} \end{bmatrix} \begin{Bmatrix} \xi_R^{(A)} \\ \xi_I^{(A)} \end{Bmatrix} = \begin{Bmatrix} 0 \\ F_I^{(A)} \end{Bmatrix} \tag{3}$$

where m is the generalized mass matrix and ω_R^2 and k_I are the generalized stiffness matrices corresponding to the interior and interface coordinates, respectively. The size of the matrices in Eq. (3) is the sum of the number of normal modes used and the number of interface dof.

2.2. Extended substructure synthesis method

For simplicity, it is assumed that the whole structure consists of two substructures (Sub-A and Sub-B), and there are no external forces applied to the interior coordinates of the substructures. If the two substructures are coupled by torsional springs located at some of the interface coordinates, the interface coordinates of each substructure can be divided into the coordinates (I_p) with torsional springs and the other coordinates (I_n). The generalized equations of motion of Sub-A and Sub-B can be expressed as

$$\begin{bmatrix} m_{RR}^{(A)} & m_{RI_n}^{(A)} & m_{RI_p}^{(A)} \\ m_{RI_n}^{(A)\mathrm{T}} & m_{I_nI_n}^{(A)} & m_{I_nI_p}^{(A)} \\ m_{RI_p}^{(A)\mathrm{T}} & m_{I_nI_p}^{(A)\mathrm{T}} & m_{I_pI_p}^{(A)} \end{bmatrix} \begin{Bmatrix} \ddot{\xi}_R^{(A)} \\ \ddot{\xi}_{I_n}^{(A)} \\ \ddot{\xi}_{I_p}^{(A)} \end{Bmatrix} + \begin{bmatrix} \omega_R^{2(A)} & 0 & 0 \\ 0 & k_{I_nI_n}^{(A)} & k_{I_nI_p}^{(A)} \\ 0 & k_{I_nI_p}^{(A)\mathrm{T}} & k_{I_pI_p}^{(A)} \end{bmatrix} \begin{Bmatrix} \xi_R^{(A)} \\ \xi_{I_n}^{(A)} \\ \xi_{I_p}^{(A)} \end{Bmatrix} = \begin{Bmatrix} 0 \\ F_{I_n}^{(A)} \\ F_{I_p}^{(A)} \end{Bmatrix} \tag{4}$$

$$\begin{bmatrix} m_{I_nI_n}^{(B)} & m_{I_nI_p}^{(B)\mathrm{T}} & m_{RI_n}^{(B)\mathrm{T}} \\ m_{I_nI_p}^{(B)} & m_{I_pI_p}^{(B)} & m_{RI_p}^{(B)\mathrm{T}} \\ m_{RI_n}^{(B)} & m_{RI_p}^{(B)} & m_{RR}^{(B)} \end{bmatrix} \begin{Bmatrix} \ddot{\xi}_{I_n}^{(B)} \\ \ddot{\xi}_{I_p}^{(B)} \\ \ddot{\xi}_R^{(B)} \end{Bmatrix} + \begin{bmatrix} k_{I_nI_n}^{(B)} & k_{I_nI_p}^{(B)} & 0 \\ k_{I_nI_p}^{(B)\mathrm{T}} & k_{I_pI_p}^{(B)} & 0 \\ 0 & 0 & \omega_R^{2(B)} \end{bmatrix} \begin{Bmatrix} \xi_{I_n}^{(B)} \\ \xi_{I_p}^{(B)} \\ \xi_R^{(B)} \end{Bmatrix} = \begin{Bmatrix} F_{I_n}^{(B)} \\ F_{I_p}^{(B)} \\ 0 \end{Bmatrix} \tag{5}$$

The compatibility equations of the interface coordinates (I_p, I_n) of the two substructures can be written as follows:

$$\{u_{I_n}^{(A)}\} = \{u_{I_n}^{(B)}\} = \{u_{I_n}\}, \ \{\xi_{I_n}^{(A)}\} = \{\xi_{I_n}^{(B)}\} = \{\xi_{I_n}\} \tag{6}$$

$$\{F_{I_p}^{(A)}\} = [K_\theta](\{u_{I_p}^{(B)}\} - \{u_{I_p}^{(A)}\}) = [K_\theta](\{\xi_{I_p}^{(B)}\} - \{\xi_{I_p}^{(A)}\} \tag{7}$$

$$\{F_{I_p}^{(B)}\} = -[K_\theta](\{u_{I_p}^{(B)}\} - \{u_{I_p}^{(A)}\}) = -[K_\theta](\{\xi_{I_p}^{(B)}\} - \{\xi_{I_p}^{(A)}\}) \tag{8}$$

where $[K_\theta]$ is a diagonal matrix of the torsional spring coefficients according to each I_p. Substitution of Eqs. (6) (7), and (8) into Eqs. (4) and (5), and coupling of these equations gives

$$\begin{bmatrix} m_{RR}^{(A)} & m_{RI_n}^{(A)} & m_{RI_p}^{(A)} & 0 & 0 \\ m_{RI_n}^{(A)\mathrm{T}} & m_{I_nI_n}^{(A)} + m_{I_nI_n}^{(B)} & m_{I_nI_p}^{(A)} & m_{I_nI_p}^{(B)\mathrm{T}} & m_{RI_n}^{(B)\mathrm{T}} \\ m_{RI_p}^{(A)\mathrm{T}} & m_{I_nI_p}^{(A)\mathrm{T}} & m_{I_pI_p}^{(A)} & 0 & 0 \\ 0 & m_{I_nI_p}^{(B)} & 0 & m_{I_pI_p}^{(B)} & m_{RI_p}^{(B)\mathrm{T}} \\ 0 & m_{RI_n}^{(B)} & 0 & m_{RI_p}^{(B)} & m_{RR}^{(B)} \end{bmatrix} \begin{Bmatrix} \ddot{\xi}_R^{(A)} \\ \ddot{\xi}_{I_n} \\ \ddot{\xi}_{I_p}^{(A)} \\ \ddot{\xi}_{I_p}^{(B)} \\ \ddot{\xi}_R^{(B)} \end{Bmatrix} + \begin{bmatrix} \omega_R^{2(A)} & 0 & 0 & 0 & 0 \\ 0 & k_{I_nI_n}^{(A)} + k_{I_nI_n}^{(B)} & k_{I_nI_p}^{(A)} & k_{I_nI_p}^{(B)} & 0 \\ 0 & k_{I_nI_p}^{(A)\mathrm{T}} & k_{I_pI_p}^{(A)} + K_\theta & -K_\theta & 0 \\ 0 & k_{I_nI_p}^{(B)\mathrm{T}} & -K_\theta & k_{I_pI_p}^{(B)} + K_\theta & 0 \\ 0 & 0 & 0 & 0 & \omega_R^{2(B)} \end{bmatrix} \begin{Bmatrix} \xi_R^{(A)} \\ \xi_{I_n} \\ \xi_{I_p}^{(A)} \\ \xi_{I_p}^{(B)} \\ \xi_R^{(B)} \end{Bmatrix} = \{0\} \tag{9}$$

The natural frequencies and eigenvectors of the combined structure with torsional springs can be easily obtained from Eq. (9), which can be applied to complex structure problems with several substructures.

2.3. Numerical example 1

To verify the extended substructure synthesis method, the free vibration of a cantilever plate is considered. The plate model-1 has two substructures coupled by a hinge section with seven torsional springs, as shown in Fig. 4. Each node has three dofs of one translation and two rotations. The torsional spring coefficient, elastic modulus, density, and Poisson ratio used for the example are $K_\theta = 1\,\mathrm{Nm/rad}$, 72 GPa, $2800\,\mathrm{kg/m^3}$, and 0.33, respectively. The frequency range of interest is chosen to be 0–500 Hz. The lowest one and seven normal modes are used to represent Sub-*A* and Sub-*B*, respectively.

By using the extended coupling method, the dynamic model of the whole structure is obtained, and the total dofs of plate model-1 can be reduced from 252 to 50. The modal parameters calculated by the present extended method are compared with those directly calculated using MSC/NASTRAN®. Table 1 gives the frequencies, error, and modal assurance criteria (MAC) [26], and Fig. 5 shows the first four fundamental mode

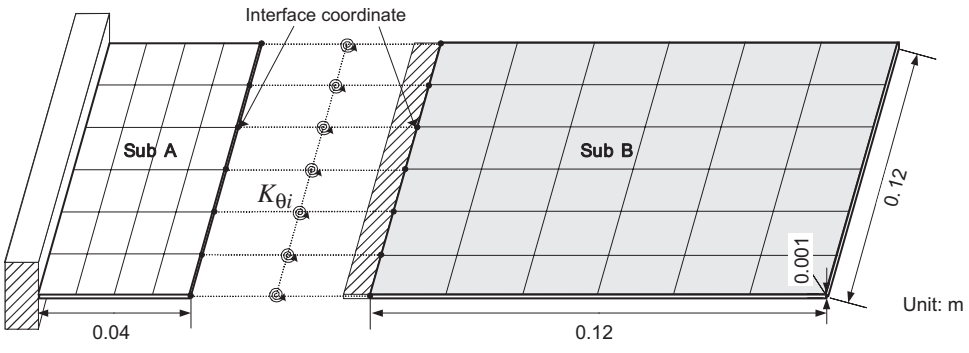

Fig. 4. A scheme of plate model-1 with two substructures and torsional springs.

Table 1
Comparison of natural frequency between NASTRAN and present method.

Frequency (Hz), error (%) and MAC				
Mode	NASTRAN	Present	Error	MAC
1	22.26	22.26	0.000	1.000
2	99.42	99.43	0.004	1.000
3	207.38	207.41	0.016	1.000
4	343.55	344.90	0.392	0.998
5	418.12	418.37	0.059	1.000
6	508.51	509.46	0.188	1.000
7	665.90	679.08	1.979	0.981
8	703.20	708.77	0.792	0.994

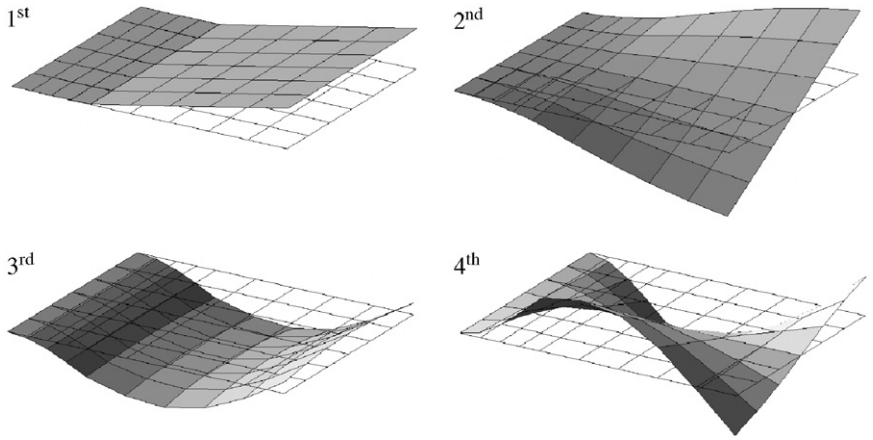

Fig. 5. First four fundamental mode shapes of plate model-1.

shapes. It is clear that the normal modes of the entire structure are accurately obtained by using the extended method.

3. Substructure synthesis for sliding mode condition

The extended substructure synthesis method described in the previous section is improved to consider the sliding mode condition. For validation of the improved method, it is applied to a three-substructure-model with structural nonlinearity of sliding lines between the substructures, and a dynamic analysis of the coupled structural model is performed for a sinusoidal external force.

3.1. Improved substructure synthesis method

In order to consider the sliding mode condition, it is assumed that there is a sliding mode condition between the substructures, as shown in Fig. 6. The interface coordinates of Sub-A and Sub-B are the guide line and the roller, respectively. The movement of the roller is free along the guide line, but restricted to the perpendicular direction to the guide line.

If the roller coordinate I_r is located between two interface coordinates, I_i and I_{i+1}, of the guide line, which are assumed to be adjacent dofs, then the generalized equations of motion of Sub-A and Sub-B can be

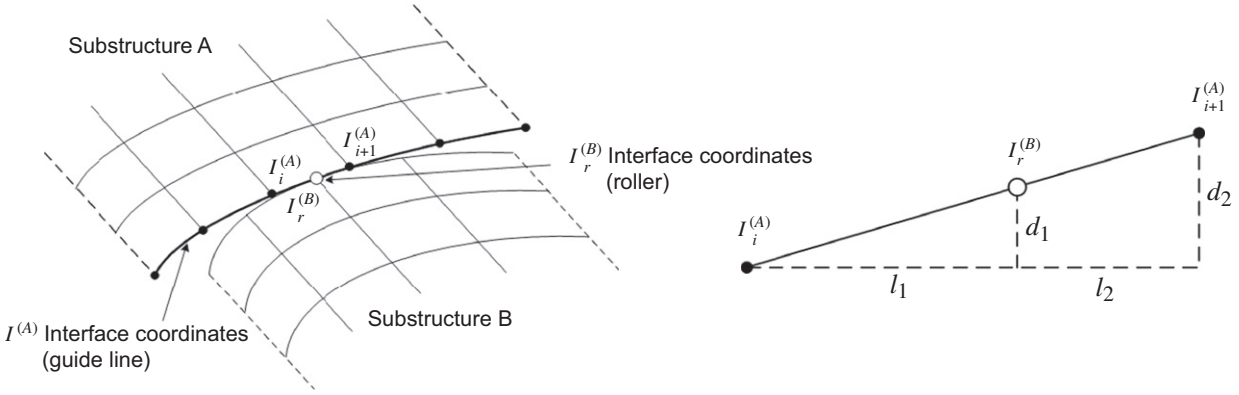

Fig. 6. A scheme of substructure analysis with sliding mode condition.

expressed in the same manner as Eqs. (4) and (5) as follows:

$$\begin{bmatrix} m_{RR}^{(A)} & m_{RI_i}^{(A)} & m_{RI_{i+1}}^{(A)} \\ m_{RI_i}^{(A)\mathrm{T}} & m_{I_iI_i}^{(A)} & m_{I_iI_{i+1}}^{(A)} \\ m_{RI_{i+1}}^{(A)\mathrm{T}} & m_{I_iI_{i+1}}^{(A)\mathrm{T}} & m_{I_{i+1}I_{i+1}}^{(A)} \end{bmatrix} \begin{Bmatrix} \ddot{\xi}_R^{(A)} \\ \ddot{\xi}_{I_i}^{(A)} \\ \ddot{\xi}_{I_{i+1}}^{(A)} \end{Bmatrix} + \begin{bmatrix} k_{RR}^{(A)} & k_{RI_i}^{(A)} & k_{RI_{i+1}}^{(A)} \\ k_{RI_i}^{(A)\mathrm{T}} & k_{I_iI_i}^{(A)} & k_{I_iI_{i+1}}^{(A)} \\ k_{RI_{i+1}}^{(A)\mathrm{T}} & k_{I_iI_{i+1}}^{(A)\mathrm{T}} & k_{I_{i+1}I_{i+1}}^{(A)} \end{bmatrix} \begin{Bmatrix} \xi_R^{(A)} \\ \xi_{I_i}^{(A)} \\ \xi_{I_{i+1}}^{(A)} \end{Bmatrix} = \begin{Bmatrix} 0 \\ 0 \\ F_{I_i}^{(A)} \\ F_{I_{i+1}}^{(A)} \\ 0 \end{Bmatrix} \tag{10}$$

$$\begin{bmatrix} m_{I_rI_r}^{(B)} & m_{RI_r}^{(B)} \\ m_{RI_r}^{(B)\mathrm{T}} & m_{RR}^{(B)} \end{bmatrix} \begin{Bmatrix} \ddot{\xi}_{I_r}^{(B)} \\ \ddot{\xi}_R^{(B)} \end{Bmatrix} + \begin{bmatrix} k_{I_rI_r}^{(B)} & k_{RI_r}^{(B)} \\ k_{RI_r}^{(B)\mathrm{T}} & k_{RR}^{(B)} \end{bmatrix} \begin{Bmatrix} \xi_{I_r}^{(B)} \\ \xi_R^{(B)} \end{Bmatrix} = \begin{Bmatrix} F_{I_r}^{(B)} + f_{I_r}^{(B)} \\ f_R^{(B)} \end{Bmatrix} \tag{11}$$

where $\{F_{I_i}^{(A)}\}$, $\{F_{I_{i+1}}^{(A)}\}$, and $\{F_{I_r}^{(B)}\}$ are the internal force vectors applied at the guide line (I_i, I_{i+1}) and the roller (I_r) by Sub-B and Sub-A, respectively. The external force vectors $\{f_{I_r}^{(B)}\}$ and $\{f_R{}^{(B)}\}$, which are generated by the external forces $\{F_R^{(B)}\}$ applied at the interior coordinates of Sub-B, can be expressed as follows:

$$\{f_{I_r}^{(B)}\} = [\Psi_C^{(B)\mathrm{T}}]\{F_R^{(B)}\} \tag{12a}$$

$$\{f_R^{(B)}\} = [\Psi_N^{(B)\mathrm{T}}]\{F_R^{(B)}\} \tag{12b}$$

For synthesis of the substructures, the compatibility equations of the interface coordinates (I_i, I_{i+1} and I_r) can be written as follows:

$$\{F_{I_i}^{(A)}\} = -\frac{l_2^A}{l_1^A + l_2^A}\{F_{I_r}^{(B)}\} = -c_i^A\{F_{I_r}^{(B)}\} \tag{13}$$

$$\{F_{I_{i+1}}^{(A)}\} = -\frac{l_1^A}{l_1^A + l_2^A}\{F_{I_r}^{(B)}\} = -c_{i+1}^A\{F_{I_r}^{(B)}\} \tag{14}$$

$$\{\xi_{I_r}^{(B)}\} = c_i^A\{\xi_{I_i}^{(A)}\} + c_{i+1}^A\{\xi_{I_{i+1}}^{(A)}\} \tag{15}$$

where l_1 and l_2 are the horizontal displacements between the interface coordinates and the roller, as shown in Fig. 6. Substitution of Eqs. (13),(14), and (15) into Eqs. (10) and (11), and coupling of these

equations gives

$$\begin{bmatrix} m_{RR}^{(A)} & & m_{RI_i}^{(A)} & m_{RI_{i+1}}^{(A)} & & 0 \\ & & & & & 0 \\ m_{RI_i}^{(A)\mathrm{T}} & & m_{I_iI_i}^{(A)} + c_i^A c_i^A m_{I_rI_r}^{(B)} & m_{I_iI_{i+1}}^{(A)} + c_i^A c_{i+1}^A m_{I_rI_r}^{(B)} & & c_i^A m_{RI_r}^{(B)} \\ m_{RI_{i+1}}^{(A)\mathrm{T}} & & m_{I_iI_{i+1}}^{(A)\mathrm{T}} + c_i^A c_{i+1}^A m_{I_rI_r}^{(B)} & m_{I_{i+1}I_{i+1}}^{(A)} + c_{i+1}^A c_{i+1}^A m_{I_rI_r}^{(B)} & & c_{i+1}^A m_{RI_r}^{(B)} \\ & & & & & 0 \\ 0 & 0 & c_i^A m_{RI_r}^{(B)\mathrm{T}} & c_{i+1}^A m_{RI_r}^{(B)\mathrm{T}} & 0 & m_{RR}^{(B)} \end{bmatrix} \begin{Bmatrix} \ddot{\xi}_R^{(A)} \\ \vdots \\ \ddot{\xi}_{I_i}^{(A)} \\ \ddot{\xi}_{I_{i+1}}^{(A)} \\ \vdots \\ \ddot{\xi}_R^{(B)} \end{Bmatrix}$$

$$+ \begin{bmatrix} k_{RR}^{(A)} & & k_{RI_i}^{(A)} & k_{RI_{i+1}}^{(A)} & & 0 \\ & & & & & 0 \\ k_{RI_i}^{(A)\mathrm{T}} & & k_{I_iI_i}^{(A)} + c_i^A c_i^A k_{I_rI_r}^{(B)} & k_{I_iI_{i+1}}^{(A)} + c_i^A c_{i+1}^A k_{I_rI_r}^{(B)} & & c_i^A k_{RI_r}^{(B)} \\ k_{RI_{i+1}}^{(A)\mathrm{T}} & & k_{I_iI_{i+1}}^{(A)\mathrm{T}} + c_i^A c_{i+1}^A k_{I_rI_r}^{(B)} & k_{I_{i+1}I_{i+1}}^{(A)} + c_{i+1}^A c_{i+1}^A k_{I_rI_r}^{(B)} & & c_{i+1}^A k_{RI_r}^{(B)} \\ & & & & & 0 \\ 0 & 0 & c_i^A k_{RI_r}^{(B)\mathrm{T}} & c_{i+1}^A k_{RI_r}^{(B)\mathrm{T}} & 0 & k_{RR}^{(B)} \end{bmatrix} \begin{Bmatrix} \xi_R^{(A)} \\ \vdots \\ \xi_{I_i}^{(A)} \\ \xi_{I_{i+1}}^{(A)} \\ \vdots \\ \xi_R^{(B)} \end{Bmatrix} = \begin{Bmatrix} 0 \\ 0 \\ c_i^A f_{I_r}^{(B)} \\ c_{i+1}^A f_{I_r}^{(B)} \\ 0 \\ f_R^{(B)} \end{Bmatrix} \tag{16}$$

Because the displacements (l_1 and l_2) and the corresponding interface coordinates (I_i and I_{i+1}) adjacent to the roller (I_r) vary according to the position of the roller, the mass and stiffness matrices of Eq. (16) have time variable nonlinear properties. By using the proposed method, a dynamic analysis of the combined structure with the nonlinearity of the sliding condition can be easily performed. The suggested approach can also be applied to complex structure problems with several substructures and guide lines. The transformation matrix from the generalized displacements to the physical displacements is

$$\begin{Bmatrix} u_R^{(A)} \\ u_I^{(A)} \\ u_I^{(B)} \\ u_R^{(B)} \end{Bmatrix} = \begin{bmatrix} \Psi_N^{(A)} & \Psi_C^{(A)} & 0 & 0 \\ 0 & I & 0 & 0 \\ 0 & 0 & I & 0 \\ 0 & 0 & \Psi_C^{(B)} & \Psi_N^{(B)} \end{bmatrix} \begin{Bmatrix} \xi_R^{(A)} \\ \xi_I^{(A)} \\ \xi_I^{(B)} \\ \xi_R^{(B)} \end{Bmatrix} \tag{17}$$

3.2. Numerical example 2

This section presents a dynamic analysis results of the three-substructure-model with sliding mode condition. Plate model-2 has three substructures, Sub-*A*, Sub-*B*, and Sub-*C*, connected to each other by sliding conditions, as shown in Fig. 7. Sub-*A* and Sub-*C* are constrained by clamped boundaries, and the interface coordinates of the substructures are guide lines. Sub-*B* is supported by two springs on both sides and has three rollers at the interface coordinates. The substructures have the same material properties used in numerical example 1, and the spring coefficient is $K = 1000\,\mathrm{N/m}$. Sub-*A* and Sub-*C* have 96 *quad-4* elements, and Sub-*B* has 144 *quad-4* elements.

Using the proposed coupling method, a reduced dynamic model of the whole structure is obtained. The frequency range of interest is chosen to be 0–500 Hz. The lowest two normal modes are used to represent Sub-*A* and Sub-*C*, respectively, and the lowest nine normal modes are used to represent Sub-*B*. The total dofs of plate model-2 can be reduced from 1365 to 92.

Because the frequency response of a nonlinear structure depends on the magnitude and the direction of external forces [27], it is not easy to determine the exact natural frequencies of the coupled plate model.

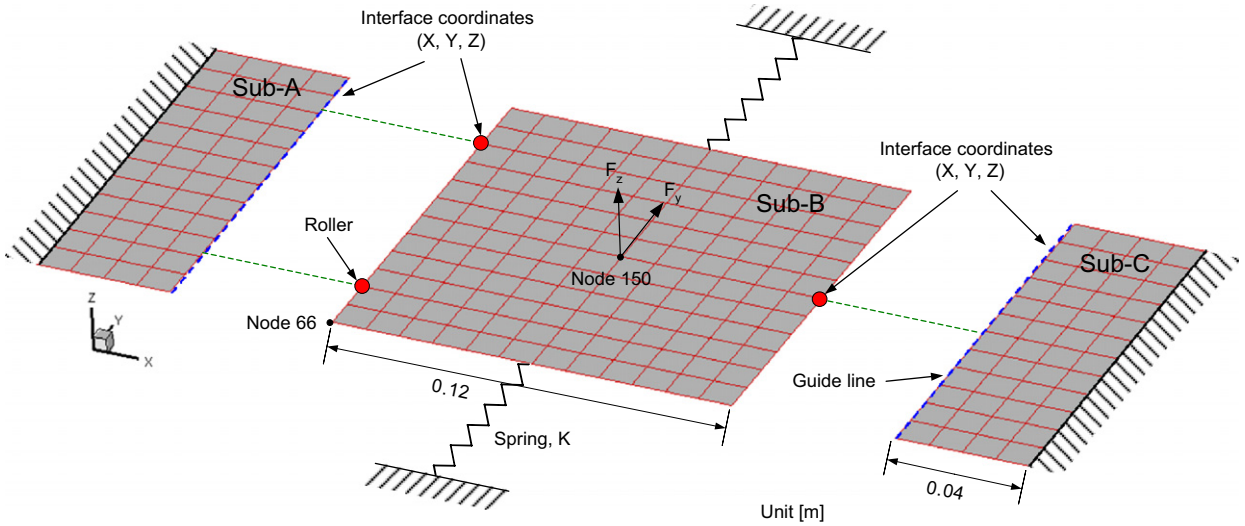

Fig. 7. A scheme of plate model-2 with three substructures and sliding mode condition.

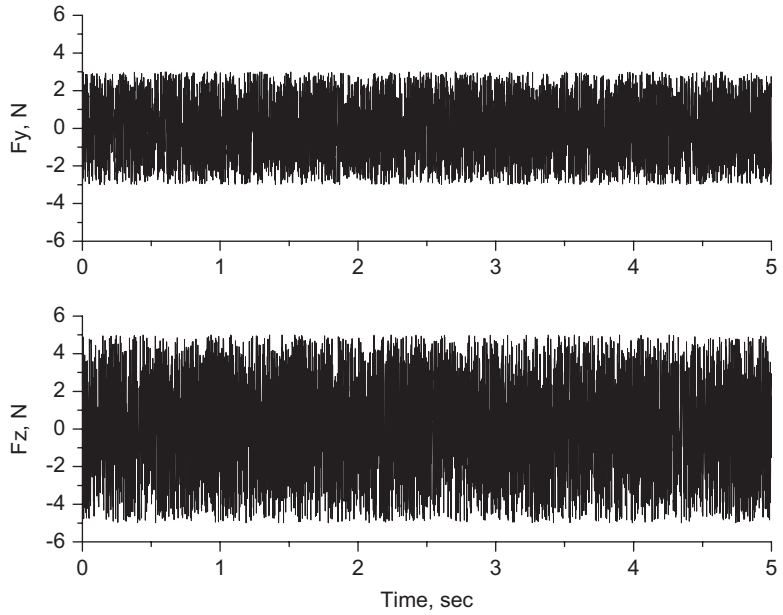

Fig. 8. Random excitation forces applied at node-150 in y and x directions.

In order to roughly investigate the natural frequencies of the coupled structure, the random excitation forces shown in Fig. 8 are applied at the center of Sub-*B* (node-150) in the y and z-directions. Fig. 9 displays the magnitude of the frequency response functions measured at the collocated node-150 in both directions for external random forces, and the lowest five modes can be found.

In order to investigate the dynamic characteristics, dynamic analyses of the reduced plate mode are performed for three kinds of external forces listed in Table 2. The excitation frequency of force-1 is the first natural frequency of 35.2 Hz in the y-direction, the frequency of force-2 is 50 Hz in both directions, and the

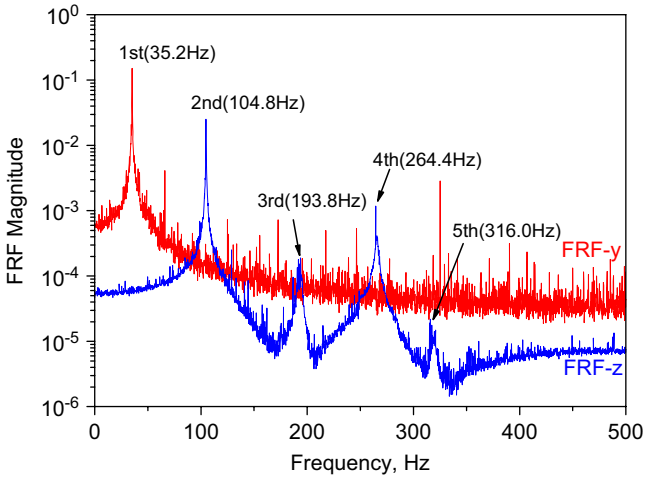

Fig. 9. Magnitudes of frequency response functions measured at node-150 for random forces.

Table 2
Excitation forces for plate model-2.

Cases	Frequency (Hz)	Excitation forces (N)
1	35.2 (first resonance)	$F_y = 0.4\sin(2\pi \times 35.2 \times t)$, $F_z = 0$
2	50.0 (~first/second resonance)	$F_y = 15\sin(2\pi \times 50 \times t)$, $F_z = 150\sin(2\pi \times 50 \times t)$
3	104.8 (~second resonance)	$F_y = 50\sin(2\pi \times 104.8 \times t)$, $F_z = 5\sin(2\pi \times 104.8 \times t)$

frequency of force-3 is 104.8 Hz, which is close to the second mode in the z-direction. The Newmark beta method is used to calculate the dynamic response with a time span of 1 ms. Fig. 10 shows the dynamic responses of the coupled model for the external forces. In Figs. 10a,c, the dynamic responses show resonance motions in the y and z-directions, respectively. The first natural mode shown in Fig. 10a is the sliding motion of the linear mass-spring system consisting of only Sub-B and the supporting springs; the dynamic response diverges in the y-direction as the time increases. The second natural mode shown in Fig. 10c is mainly the resonance motion in the z-direction, but the motion is coupled with the sliding motion in the y-direction. Therefore, the resonance motion is nonlinear and converges in the z-direction. The dynamic responses for excitation force-2 are shown in Fig. 10b and Fig. 11, which clearly verify the dynamic connectivity between the substructures. From the results, it is noted that the excitation frequencies and the nonlinear dynamic characteristics are clearly shown in the responses of the coupled model.

4. Tilting structure with sliding mode condition

A reduced dynamic model of a tilting structure, consisting of sledge and base frames that are connected by the sliding mode condition, is established using the proposed coupling method. The dynamic responses of the coupled model for sinusoidal external forces are then analyzed to investigate the nonlinear dynamic characteristics of the tilting structure.

4.1. Tilting structure

The tilting structure of a tilting train is attached on the roof of the carriage and supports the pantograph such that it can maintain the horizontal position of the pantograph while traveling on curved lines. Shown in

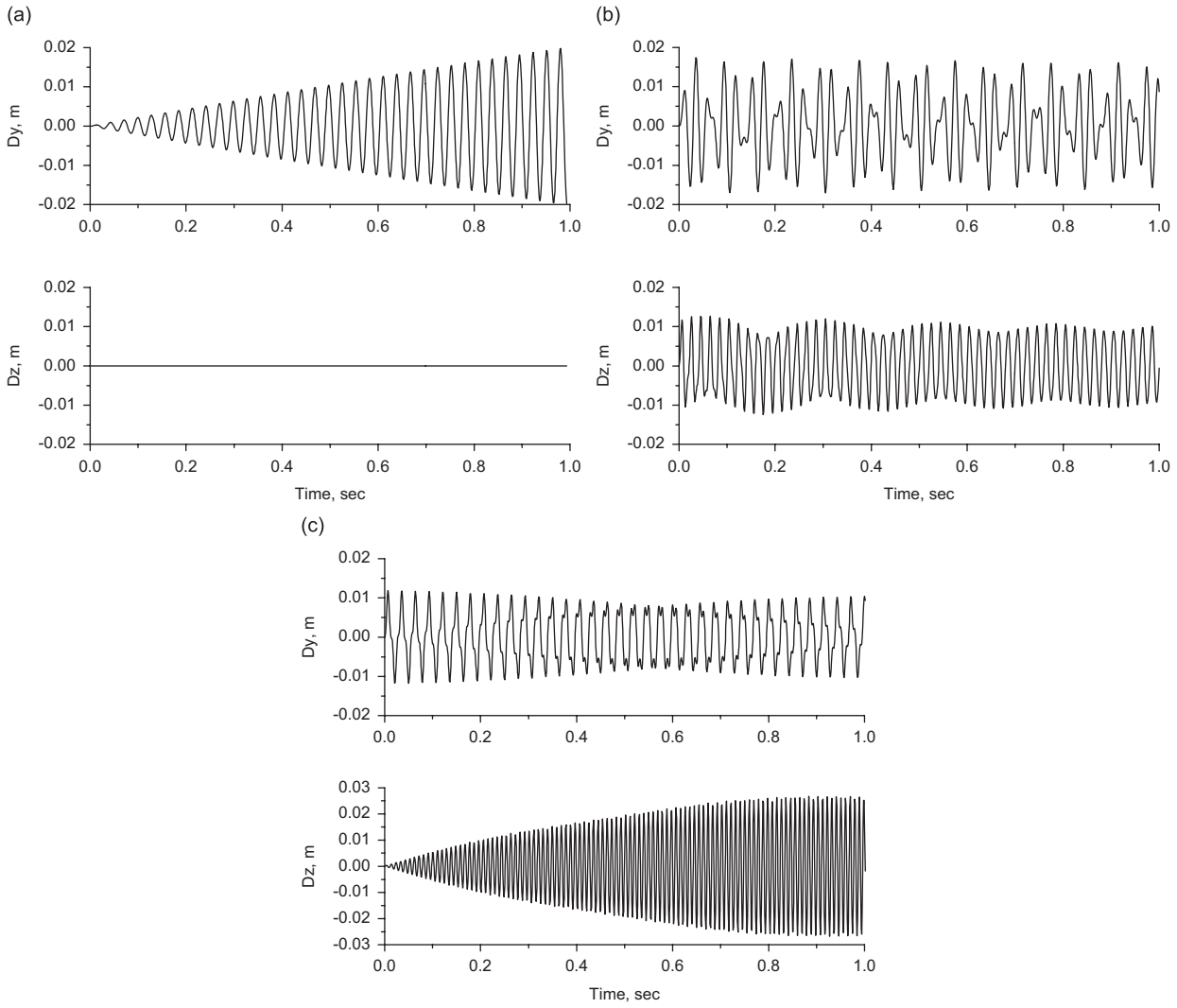

Fig. 10. Dynamic responses of plate model-2 measured at node-150: (a) excitation force-1; (b) excitation force-2; and (c) excitation force-3.

Fig. 12 is the tilting structure for a roof mounted active pantograph, which consists of base and sledge frames connected with each other under the sliding mode condition. The weights of the base and sledge frames are 184 and 127 kg, respectively. The sledge frame has three roller sets restricted to follow two guide lines of the base frame fixed on the roof using 10 fixing points. The maximum displacement of the rollers on the guide lines is limited to ± 322.5 mm along the guide lines. The frame is connected by two main springs attached on both sides of the base frame to maintain its neutral position without external forces, and is driven by the main belt, which transmits the driving force from the electric motor to the frame.

In order to establish a reduced dynamic model of the tilting structure, the structure is divided into two substructures, substructure *A* (base frame) and substructure *B* (sledge frame). The material of the frames is SS400 and its properties are listed in Table 3. MSC/PARTRAN® is used to construct the finite element models of the substructures, as shown in Fig. 13a. Sub-*A* has 512 *tria-3* and *quad-4* elements, and Sub-*B* has 259 *tria-3* and *quad-4* elements. The total dofs of Sub-*A* and Sub-*B* are 2683 and 1422, respectively. The frequency range of interest of the tilting structure is 0–100 Hz. Thus, the first seven and nine modes are used to

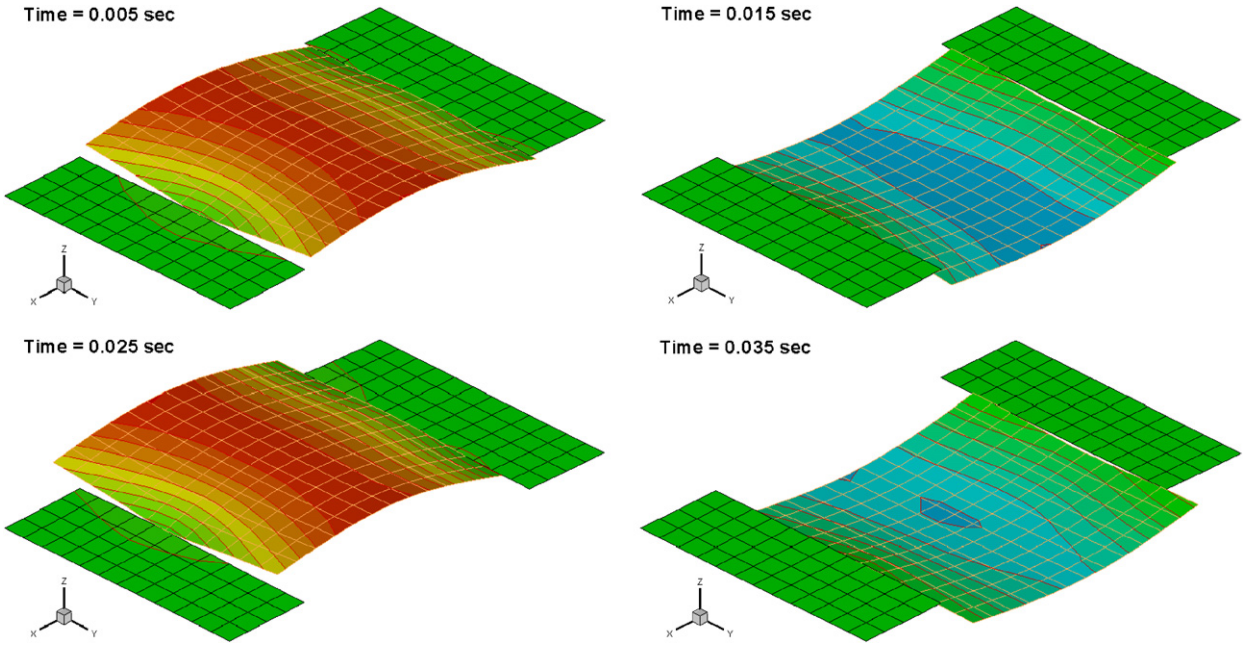

Fig. 11. Dynamic response motions of plate model-2 for excitation force-2.

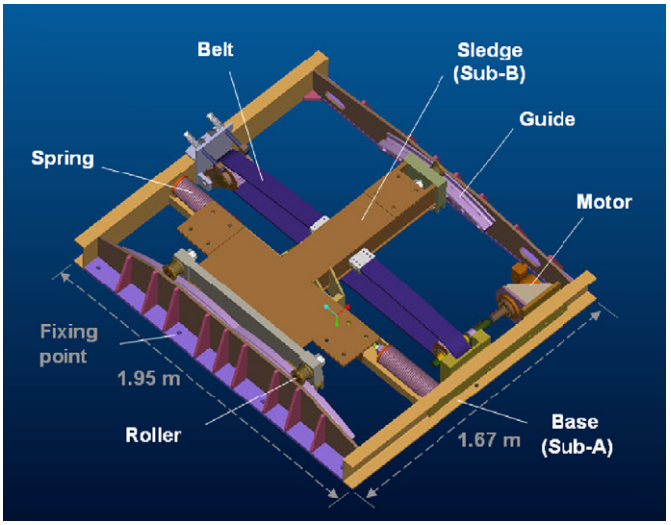

Fig. 12. 3D CAD model of the tilting structure.

Table 3
Material properties of Sub-*A* and Sub-*B*.

SS400	
Density	7.85 g/cm^3
Tensile ultimate strength	400–500 Mpa
Tensile yield strength	250 Mpa
Modulus of elasticity	200 Gpa
Poisson ratio	0.26
Shear modulus	79.3 Gpa

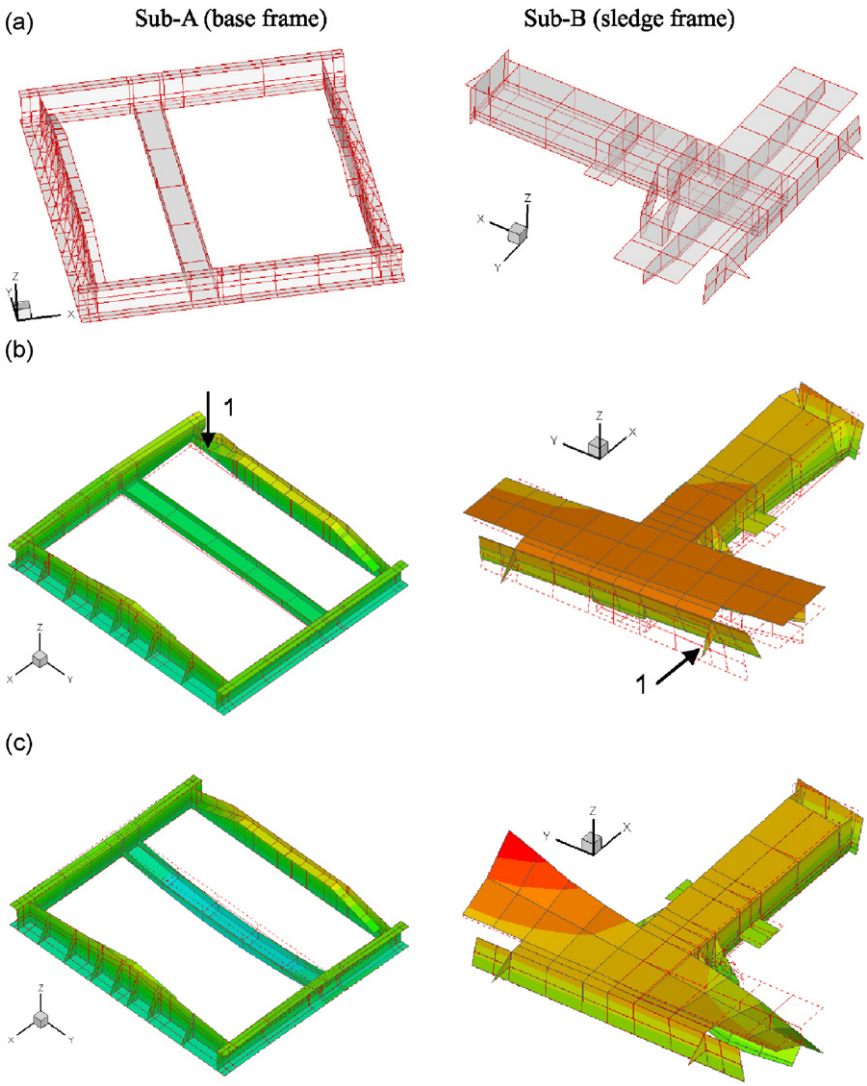

Fig. 13. Substructure models and mode shapes: (a) finite element models, (b) constraint modes, (c) first normal modes (Sub-*A*: 55.89 Hz, Sub-*B*: 80.82 Hz).

represent the base and sledge frames, respectively, as shown in Fig. 13c. By using the proposed coupling method, a reduced dynamic model of the tilting structure is established as shown in Fig. 14. The total dofs of the tilting structure can be reduced from 4105 to 100. The substructures are connected by the sliding mode conditions in the interface coordinates. The main springs are represented by the springs and dampers, and their coefficients are 5000 N/m and 30 N s/m, respectively.

4.2. Dynamic characteristics

The dynamic characteristics of the coupled model are investigated through dynamic analyses of the tilting structure excited by three kinds of external forces listed in Table 4. The excitation frequency of force-1 is 0.99 Hz, which is near to the first natural frequency of the sledge frame in the *y*-direction, the frequency of force-2 is 19.8 Hz, which is near to the second natural frequency in the *x*-direction, and these two excitation frequencies are applied simultaneously in both directions in force-3.

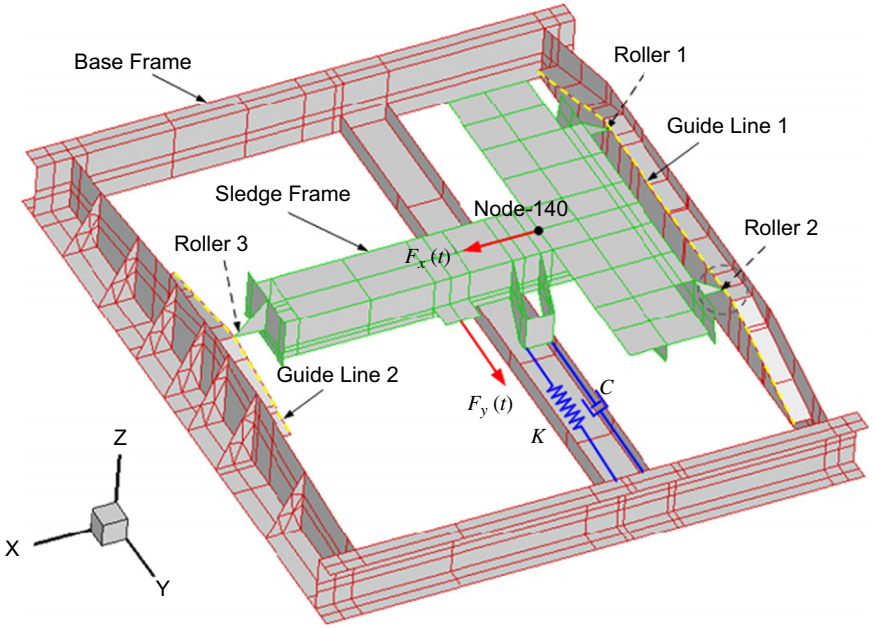

Fig. 14. Coupled model of the tilting structure and applied forces.

Table 4
Excitation forces for tilting structure.

Cases	Excitation forces (N)
1	$F_x = 0$, $F_y = 100 \times \sin(2\pi \times 0.99 \times t)$, $F_z = 0$
2	$F_x = 3000 \times \sin(2\pi \times 19.8 \times t)$, $F_y = 0$, $F_z = 0$
3	$F_x = 3000 \times \sin(2\pi \times 19.8 \times t)$, $F_y = 100 \times \sin(2\pi \times 0.99 \times t)$, $F_z = 0$

Fig. 15 shows the dynamic displacements of node-140, the center of the sledge frame. The resonance motion of the sledge frame in the y-direction is shown in Fig. 15a. The horizontal displacement of the sledge frame diverges in the y-direction as the time increases, and the vertical displacement oscillates with the horizontal position of the sledge frame due to the sliding mode condition. Fig. 15b shows the dynamic responses of the sledge frame for force-2. The displacements in the x and z-axes increase rapidly but converge in both directions as the time increases. Resonant beating phenomena can also be found at less than 5 s. Fig. 15c shows the dynamic responses for force-3. The displacements in the x, y, and z-directions increase gradually, and then decrease as the time increases, similar to the resonant beating phenomenon. Although the maximum magnitude of the displacement in the x-direction is restricted to 19 mm for force-2, it increases up to 102 mm for force-3 because the motion is coupled with sliding motion of the sledge frame in the y-direction. The dynamic response motions for excitation force-3 are shown in Fig. 16, which clearly verify the dynamic connectivity between the substructures and the sliding mode condition.

From the results, it is noted that because of the nonlinearity of the sliding mode condition, the resonant frequencies and responses of the tilting structure vary according to the position of the sledge and the magnitude of external forces. The displacement in the z-direction, which mostly affects the pantograph in its power collection, can be resonated by external forces in the x and y-directions. Therefore, these nonlinear effects should be considered in the analyses of the dynamic responses of the pantograph tilting system in order to assure not only efficiency of the power collection but also the safety of the tilting train.

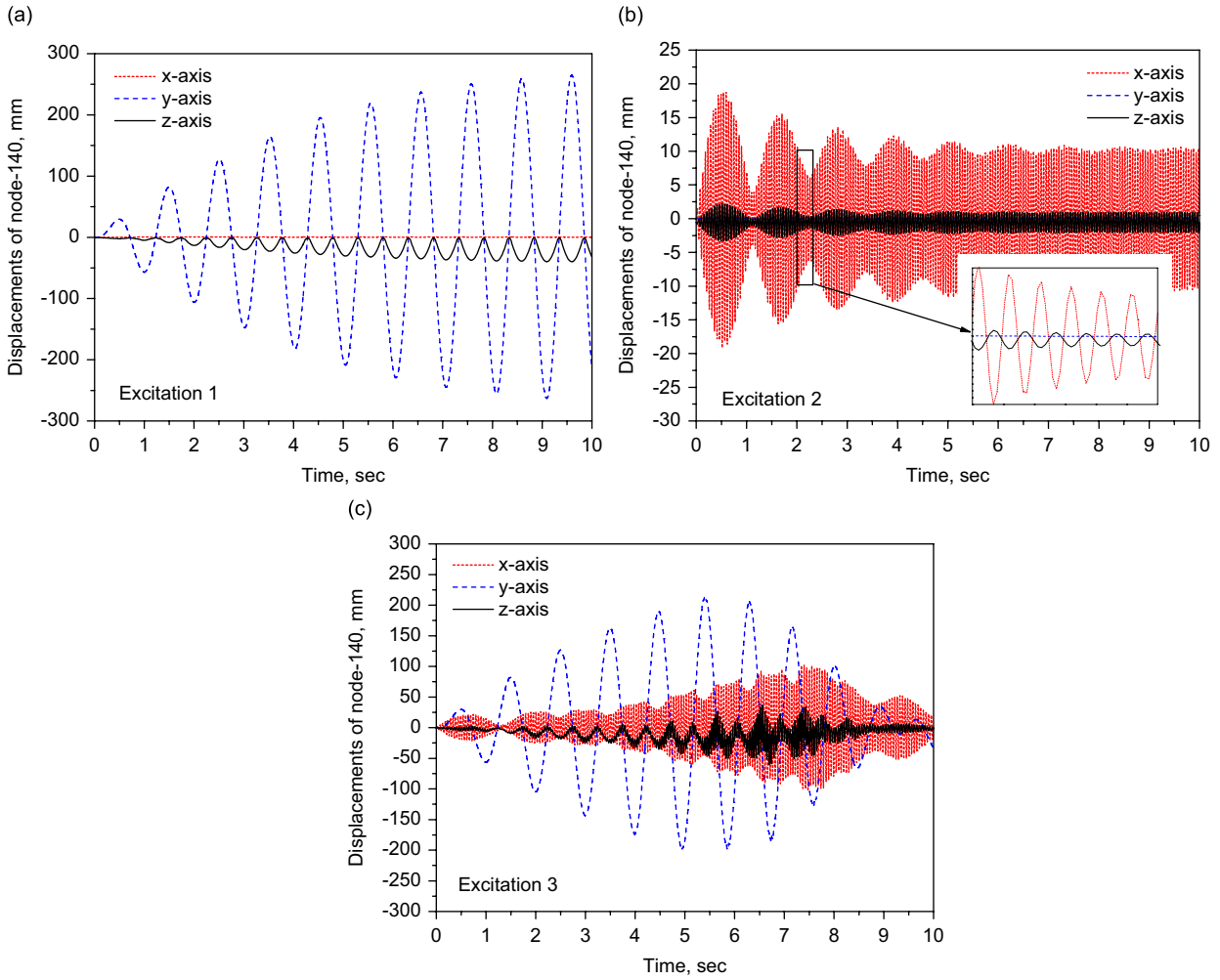

Fig. 15. Dynamic responses of the tilting structure measured at node-140: (a) excitation force-1; (b) excitation force-2; and (c) excitation force-3.

5. Conclusions

The CMS method is improved to construct a dynamic model of nonlinear structures with the sliding mode condition. For validation of the extended coupling method, numerical plate model-1 consisting of two substructures that are connected by seven torsional springs is synthesized, and its modal parameters are compared with analysis results obtained by MSC/NASTRAN®. An improved coupling method is then proposed to consider the structural nonlinearity of the sliding mode condition. The improved method is applied to numerical plate model-2 consisting of three substructures that are connected by the sliding mode condition, and the coupled structural model is verified by dynamic results. Finally, using the proposed coupling method, a reduced nonlinear model of the tilting structure consisting of sledge and base frames is established. Dynamic analyses of the tilting structure are performed for resonant external forces, and the nonlinear dynamic characteristics are investigated. The analysis results show that the improved coupling method is effectively applicable to the structural analyses of nonlinear structures with not only hinge joints but also the sliding mode condition. The additional numerical or experimental validations of the present coupling method are subjects of future work.

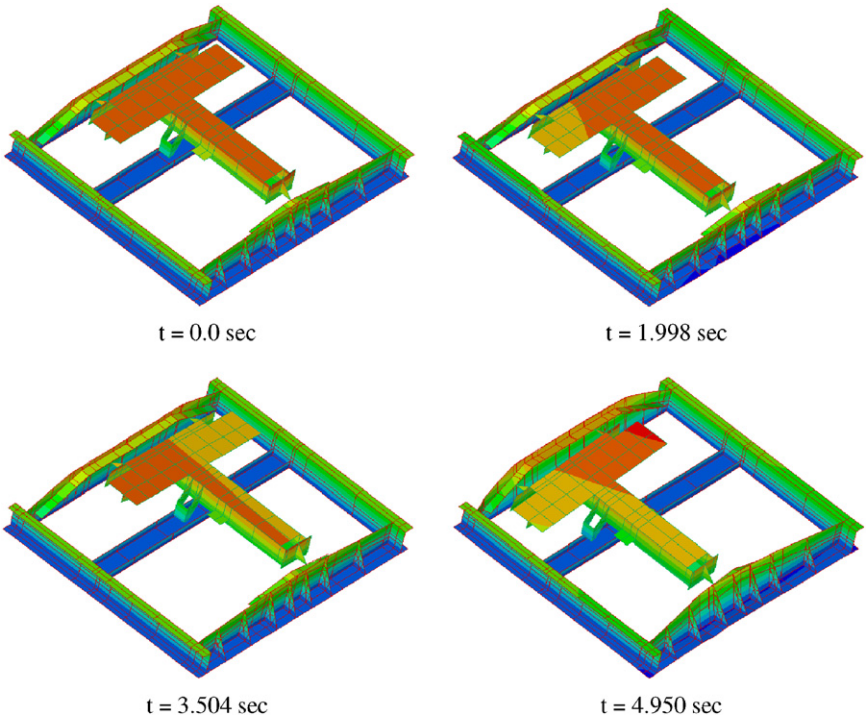

Fig. 16. Dynamic response motions of the tilting structure for excitation force-3.

Acknowledgments

This research was supported by the Korea Railroad Research Institute (KRRI) and Yujin Machinery Ltd. This support is gratefully acknowledged. The first author would like to thank the Brain Korea 21 Project in 2006.

References

[1] J.S. Bae, D.K. Kim, W.H. Shin, I. Lee, S.H. Kim, Nonlinear aeroelastic analysis of a deployable missile control fin, *Journal of Spacecraft and Rockets* 41 (2) (2004) 264–271.
[2] R. Schneider, Pantograph for tilting trains, *Current Collection for High Speed Trains Seminar, IEE,* (1998) 2/1–2/6.
[3] B.A. Hunn, A method of calculating the normal modes of an aircraft, *Quarterly Journal of Mechanics* 8 (1955) 38–58.
[4] W.C. Hurty, Dynamic analysis of structural systems using component modes, *AIAA Journal* 3 (1965) 678–685.
[5] R.R. Craig, M. Bampton, Coupling of structures for dynamic analyses, *AIAA Journal* 6 (7) (1968) 1313–1319.
[6] R.R. Craig, C.-J. Chang, Free-interface methods of substructure coupling for dynamic analysis, *AIAA Journal* 14 (11) (1976) 1633–1635.
[7] R.R. Craig, C-J. Chang, On the use of attachment modes in substructure coupling for dynamic analysis, *Proceedings of the AIAA/ASME 18th Structures, Structure Dynamics & Materials Conference*, AIAA Paper, Vol.77–405, 1977, pp. 89–99.
[8] A.L. Hale, L. Meirovitch, A general substructure synthesis method for the dynamic simulation of complex structure, *Journal of Sound and Vibration* 69 (2) (1980) 309–326.
[9] L. Meirovitch, A.L. Hale, A general dynamic synthesis for structures with discrete substructures, *Journal of Sound and Vibration* 85 (4) (1982) 445–457.
[10] M. Karpel, M. Newman, Accelerated convergence for vibration modes using the substructure coupling method and fictitious coupling masses, *Israel Journal of Technology* 13 (1975) 55–62.
[11] M. Karpel, Efficient vibration mode analysis of aircraft with multiple external store configuration, *Journal of Aircraft* 25 (8) (1999) 747–751.
[12] M. Karpel, D.M. Raveh, Fictitious mass element in structure dynamics, *AIAA Journal* 34 (3) (1996) 607–613.
[13] F. Bourquin, F. d'Hennezel, Numerical study of an intrinsic component mode synthesis method, *Computer Methods in Applied Mechanics and Engineering* 97 (1) (1992) 49–76.

[14] D.M. Tran, Component mode synthesis methods using interface modes. Application to structures with cyclic symmetry, *Computers & Structures* 79 (2) (2001) 209–222.
[15] R. Bladh, C. Pierre, M.P. Castanier, Numerical instability of classical free-interface component mode synthesis techniques, *AIAA Journal* 41 (8) (2003) 1621–1624.
[16] P. Apiwattanalunggarn, S.W. Shaw, C. Pierre, Component mode synthesis using nonlinear normal modes, *Nonlinear Dynamics* 41 (1/3) (2005) 17–46.
[17] D.K. Kim, J.S. Bae, I. Lee, J.H. Han, Dynamic characteristics and model establishment of deployable missile control fin with nonlinear hinge, *Journal of Spacecraft and Rockets* 42 (1) (2005) 66–77.
[18] A. Shanmugam, C. Padmanabhan, A fixed-free interface component mode synthesis method for rotordynamic analysis, *Journal of Sound and Vibration* 297 (3/5) (2006) 664–679.
[19] G. Poetsch, J. Evans, R. Meisinger, W. Kortum, W. Baldauf, A. Veitl, J. Wallaschek, Pantograph/catenary dynamics and control, *Vehicle System Dynamics* 28 (2/3) (1997) 159–195.
[20] A. Balestrino, O. Bruno, A. Landi, L. Sani, Innovation solutions for overhead catenary–pantograph system: wire actuated control and observed contact force, *Vehicle System Dynamics* 33 (2) (2000) 69–89.
[21] A. Levant, A. Pisano, E. Usai, Output-feedback control of the contract-force in high-speed-train pantographs, *Proceedings of the 40th IEEE Conference on Decision and Control*, Vol. 2, 2001, pp. 1831–1836.
[22] T.X. Wu, M.J. Brennan, Dynamic stiffness of a railway overhead wire system and its effect on pantograph–catenary system dynamics, *Journal of Sound and Vibration* 219 (3) (1999) 483–502.
[23] M. Arnold, B. Simeon, Pantograph and catenary dynamics: a benchmark problem and its numerical solution, *Applied Numerical Mathematics* 34 (4) (2000) 345–362.
[24] B. Simeon, M. Arnold, Coupling DAEs and PEDs for simulating the interaction of pantograph and catenary, *Mathematical and Computer Modelling of Dynamic Systems* 6 (2) (2000) 129–144.
[25] J.-H. Seo, S.-W. Kim, I.-H. Jung, T.-W. Park, J.-Y. Mok, Y.-G. Kim, J.-B. Chai, Dynamic analysis of a pantograph–catenary system using absolute nodal coordinates, *Vehicle System Dynamics* 44 (8) (2006) 615–630.
[26] R.J. Allemang, D.L. Brown, A correlation coefficient for modal vector analysis, *Proceedings of first International Modal Analysis Conference*, 1982, pp. 110–116.
[27] A.H. Nayfeh, D.T. Mook, *Nonlinear Oscillations*, Wiley, NJ, 1979.